Phonon interference and thermal conductance reduction in atomic-scale metamaterials

Haoxue Han,[1,2] Lyudmila G. Potyomina,[3] Alexandre A. Darinskii,[4] Sebastian Volz,[1,2] and Yuriy A. Kosevich[1,2,5,*]

[1]*CNRS, UPR 288 Laboratoire d'Energétique Moléculaire et Macroscopique, Combustion (EM2C),*
Grande Voie des Vignes, 92295 Châtenay-Malabry, France
[2]*Ecole Centrale Paris, Grande Voie des Vignes, 92295 Châtenay-Malabry, France*
[3]*Department of Physics and Technology, National Technical University "Kharkiv Polytechnic Institute",*
Frunze Street 21, Kharkiv 61002, Ukraine
[4]*Institute of Crystallography, Russian Academy of Sciences, Leninskii Avenue 59, Moscow 119333, Russia*
[5]*Semenov Institute of Chemical Physics, Russian Academy of Sciences, Kosygin Street 4, Moscow 119991, Russia*

We introduce and model a three-dimensional (3D) atomic-scale phononic metamaterial producing two-path phonon interference antiresonances to control the heat flux spectrum. We show that a crystal plane partially embedded with defect-atom arrays can completely reflect phonons at the frequency prescribed by masses and interaction forces. We emphasize the predominant role of the second phonon path and destructive interference in the origin of the total phonon reflection and thermal conductance reduction in comparison with the Fano-resonance concept. The random defect distribution in the plane and the anharmonicity of atom bonds do not deteriorate the antiresonance. The width of the antiresonance dip can provide a measure of the coherence length of the phonon wave packet. All our conclusions are confirmed both by analytical studies of the equivalent quasi-1D lattice models and by numerical molecular dynamics simulations of realistic 3D lattices.

Two-photon interference can result in a total cancellation of the photon output because of the coalescence of the two single photons, which was first observed by Hong *et al.* [1]. This interference effect occurs because two possible photon paths interfere destructively, which produces the famous Hong-Ou-Mandel (HOM) dip in the detection probability of the output photons. The HOM dip has since then been demonstrated in both the optical [2,3] and microwave [4] regime. In particular, two-photon destructive interference was recently demonstrated in a 3D optical metamaterial [5]. A similar destructive interference effect which results in a total reflection can be also realized in a phonon system. For the sound waves, the two-path phonon interference antiresonance was first described in Ref. [6], where the anomalous zero-transmission and total absorption of long-wavelength acoustic waves in a crystal with 2D (planar) defect were related with the *destructive interference* between the two possible phonon paths: through the nearest-neighbor bonds and through the non-nearest-neighbor bonds which couple directly crystal layers adjacent to the defect atomic plane.

Constant endeavor has been devoted to the precise control of heat conduction. Recent efforts concentrated on reducing the thermal conductivity κ via nanostructured materials with superlattices [7,8] and embedded nanoparticles [9–11]. Most works attributed the reduction of κ to the decreased phonon lifetime and thus the mean-free path (MFP), which belong to the particle description of heat conduction. However, the role of destructive phonon interference in the reduction of κ is much less understood in the wave picture of thermal transport.

In this Rapid Communication we introduce and model a realistic 3D atomic-scale phononic metamaterial that allows for manipulating the flow of thermal energy. Two-path phonon interference is generated by exploiting the phonon reflection on internal interfaces embedded with defect-atom arrays. The 2D planar defects force phonons to propagate through two paths: through unperturbed (matrix) and perturbed (defect) interatomic bonds [6,12]. The resulting phonon interference yields transmission antiresonance (zero-transmission dip) in the spectrum of short-wavelength phonons that can be controlled by the masses, force constants, and 2D concentration of the defect atoms. Our results show that the patterning of the defect-atom arrays can lead to a new departure in thermal energy management [13], offering potential applications in thermal filters [14], thermal diodes [15], and thermal cloaking [16–18].

An atomic presentation of the 3D phononic metamaterial with a face-centered cubic (FCC) lattice including a 2D array of heavy defect atoms is depicted in Fig. 1(a). The defect-atom arrays are distributed periodically or randomly in the defect crystal plane with different filling fractions f_d. When the defects do not fill entirely the defect plane, phonons have two paths to cross such an atom array as shown in Fig. 1(a), whereas the phonon path through the host atoms is blocked when the defect layer is constituted by a uniform impurity-atom array, 100%-packed with impurity atoms. Two types of atomic metamaterials were studied using realistic interatomic potentials: a FCC lattice of Argon (Ar) where the defects are heavy isotopes and a diamond lattice of Si with Germanium (Ge) atoms as the defects. The interactions between Ar atoms are described by the Lennard-Jones potential [19]. The covalent Si:Si/Ge:Ge/Si:Ge interactions are modeled by the Stillinger-Weber (SW) potential [20]. To probe the phonon transmission, the molecular dynamics (MD) based phonon wave packet (WP) method [21] was used to provide the per-phonon-mode energy transmission coefficient. The spatial width l (coherence length) of the WP is taken much larger than the wavelength λ_c of the WP central frequency, corresponding

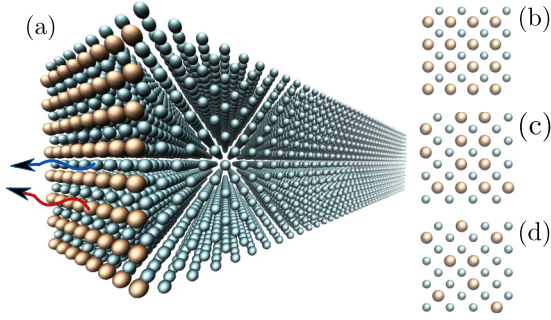*Corresponding author: yukosevich@gmail.com

FIG. 1. (Color online) (a) A phononic metamaterial with a FCC lattice containing a defect plane in which an impurity-atom array is embedded. The red and blue curve refer to the phonon path through the impurity atom bonds and through the host atom bonds, respectively. The presence of the two possible phonon paths can result in the "two-path phonon interference" antiresonance. The brown atoms are defect atoms and the green ones are the atoms of the host lattice. (b) The defect atoms have a periodic distribution with $f_d = 50\%$. Randomly distributed defect atoms with (c) $f_d = 37.5\%$ and (d) 25% in the defect plane.

to the plane-wave approximation. All the MD simulations were performed with the LAMMPS code package [22].

The transmission coefficient $\alpha(\omega)$ of the WP with $l = 20\lambda_c$, retrieved from MD simulations of an Ar metamaterial, is presented in Fig. 2. The incident phonons undergo a total reflection on the defect layer at the antiresonance frequency ω_R. Phonon transmission spectra display an interference antiresonance profile since the two phonon paths interfere destructively at ω_R, analogous to the two-photon interference which results in the HOM dip [1,5]. A total transmission at ω_T
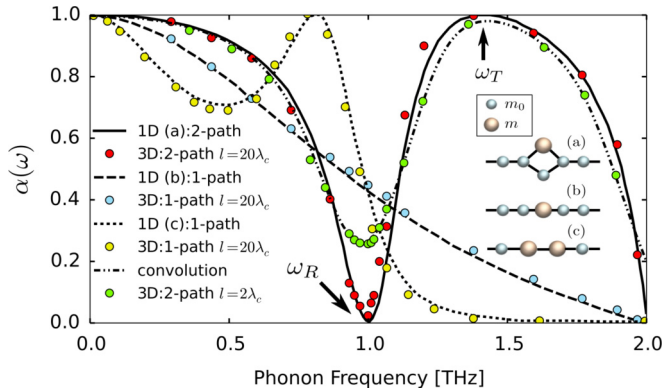

FIG. 2. (Color online) Spectra of phonon energy transmission coefficient predicted by equivalent quasi-1D model (solid and dashed lines) and by MD simulations (symbols) of a 3D Ar metamaterial with planar defect containing heavy impurities, with mass $m = 3m_0$. Dashed-dotted line is the convolution of $\alpha(\omega)$ in Eq. (1) with a Gaussian WP with $l = 2\lambda_c$. Red, blue, and yellow symbols represent transmission of WP with $l = 20\lambda_c$ through the two paths, one path with a single and two successive layers of defect atoms, respectively; green symbols represent transmission of WP with $l = 2\lambda_c$ through two paths. Inset: Three possible quasi-1D lattice models describing phonon propagation through the lattice region containing the local defect. Black sticks between the atoms represent atom bonds. In the case of the Ar lattice, the coefficients in Eq. (1) are $\omega_R = 1.0$, $\omega_T = 1.4$, $\omega_{max} = 2.0$, and $C = 0.25$.

follows the interference antiresonance, which is reminiscent of the Fano resonance [23]. For a uniform defect-atom array, the zero-transmission antiresonance profile will be totally suppressed and replaced by a monotonous decay of transmission with frequency. In the latter case, only the phonon path through the defect atoms is accessible.

We emphasize that the second phonon path is indispensable to the emergence of the zero-transmission dip, which cannot be sufficiently described by the Fano resonance. We clarify this by studying the phonon transmission through two successive uniform defect arrays, where a local resonant minimum is observed instead of a zero-transmission dip in Fig. 2. This transmission minimum and the following maximum satisfy together the Fano-resonance condition [23] of a discrete state resonating with its continuum background, but no zero-transmission dip occurs because of the absence of the second phonon path [6,12,24]. This resonance can be considered as phonon analogy of the Fabry-Pérot resonance in optics, which requires only a single phonon path. Therefore this clearly corroborates the two-path destructive interference nature of the zero-transmission dip in $\alpha(\omega)$.

To further understand the phonon antiresonances caused by the interference between two phonon channels, we use an equivalent model of a monatomic quasi-1D lattice of coupled harmonic oscillators [12], depicted in the inset in Fig. 2. In model (a), phonons propagate through two paths: through the host atom bonds, and through those of the impurity atoms, whereas in models (b) and (c), only the second channel remains open. The model (a) gives the energy transmission coefficient for plane wave:

$$\alpha(\omega) = \frac{\left(\omega^2 - \omega_R^2\right)^2\left(\omega_{max}^2 - \omega^2\right)}{\left(\omega^2 - \omega_R^2\right)^2\left(\omega_{max}^2 - \omega^2\right) + C\omega^2\left(\omega^2 - \omega_T^2\right)^2}, \quad (1)$$

where $\omega_{R,T}$ are the frequencies of the reflection and transmission resonances, and ω_{max} is the maximal phonon frequency for a given polarization, $\omega_R < \omega_T < \omega_{max}$. C is a real positive coefficient given by the atomic masses, force constants, and f_d; $C = 0$ for $f_d = 0$. The ω_R frequency exists only in the presence of an additional channel which is open for wave propagation through the bypath around the defect atom; see inset (a) in Fig. 2. As follows from Eq. (1) and Fig. 2, $\alpha(\omega_R) = \alpha(\omega_{max}) = 0$ and $\alpha(\omega_T) = \alpha(0) = 1$. In the transmission of a narrow WP with $l = 2\lambda_c$, given by the convolution of $\alpha(\omega)$ for plane wave from Eq. (1) with a Gaussian WP in frequency domain with $l = 2\lambda_c$, the interference effect is weakened by a large number of frequency components when the plane-wave approximation ($l \gg \lambda_c$) is broken and the transmission at ω_R is not zero any more, i.e., $\alpha(\omega_R) > 0$, which is the case also in [1]. As depicted in Fig. 2, an excellent agreement in transmission coefficients is demonstrated between the equivalent quasi-1D model provided by Eq. (1) and the MD simulations of the 3D atomic-scale phononic metamaterial with the use of realistic interatomic potential.

In a lattice with atomic impurities, the substituent atoms scatter phonons due to differences in mass and/or bond stiffness. Since no bond defect was introduced, the loci of the resonances are only determined by the mass of the isotope atoms. As the defect atoms get heavier, the two-path phonon interference antiresonance becomes more pronounced in terms
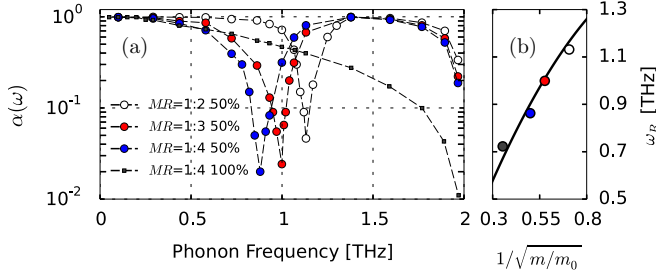
FIG. 3. (Color online) (a) Spectra of phonon transmission coefficient α of longitudinal acoustic mode in the phononic metamaterial, which consists of 2D array of periodically alternating isotopes with different mass ratio (MR) m/m_0 with $f_d = 50\%$ in a 3D Ar lattice. Black squares refer to $f_d = 100\%$ in the defect plane in comparison with the $f_d = 50\%$ case. Dashed lines are a guide to the eye. (b) Isotopic shift of the two-path phonon interference resonance versus the mass ratio m/m_0. Symbols present the resonances from MD simulations of a 3D lattice and solid line shows the analytical prediction of the equivalent quasi-1D lattice model given by Eq. (2).

of phonon attenuation depth and width, and demonstrates a redshift in the phonon transmission spectrum thus impeding the long-wavelength phonons, as shown in Fig. 3(a). The equivalent quasi-1D lattice model gives the following expression for the frequency of the transmission dip:

$$\omega_R = \omega_{\max}/\sqrt{m/m_0 + 1}, \qquad (2)$$

where m and m_0 refer to the atomic mass of the defect and host atom, $m > m_0$. The transmission resonance at $\omega = \omega_T$ is much less sensitive to the defect mass since it is largely determined by the mass of the host atom. As depicted in Fig. 3(b), the spectral positions of the interference resonances ω_R are again in an excellent agreement with the analytical prediction of the equivalent quasi-1D lattice model given by Eq. (2).

In Fig. 3(a), the transmission spectra for longitudinal phonons across the uniform defect-atom array is plotted to be compared with that of the 50%-filled defect-atom array. At the two-path interference antiresonance frequency ω_R, an array of 50% defect atoms has a transmittance two orders of magnitude smaller than that of a uniform defect-atom array. The difference between the very strong phonon reflection on a 50%-filled defect array and the high phonon transmission across a uniform defect array can result in a counterintuitive effect: an array of segregated impurity atoms can scatter more thermal phonons than an array with a uniform distribution of heavy isotopes. This anomalous phonon transmission phenomenon in molecular systems can find its acoustic counterpart in macroscopic structures [12,25,26]. In Ref. [25], perforated plates were proved to shield ultrasonic acoustic waves in water much more effectively than uniform plates. Liu *et al.* [26] managed to break the mass-density law for sonic transmission by embedding high-density spheres coated with a soft material in a single layer of a stiff matrix.

We calculate the interfacial thermal conductance G by following the Landauer-like formalism [27]:

$$G = \int \sum_{\nu} \hbar\omega(\mathbf{k},\nu) v_{g,z}(\mathbf{k},\nu) \alpha(\omega) \frac{\partial}{\partial T} n_{BE}(\omega,T) \frac{d\mathbf{k}}{(2\pi)^3}, \quad (3)$$
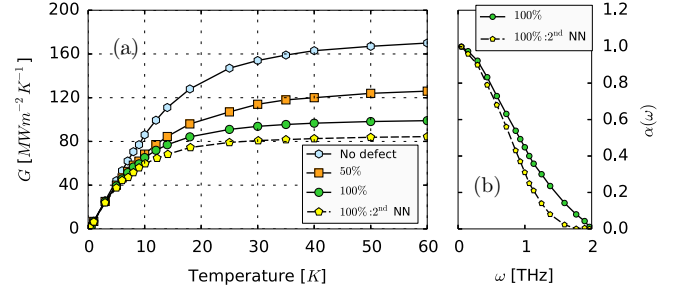

FIG. 4. (Color online) (a) The temperature-dependent interfacial thermal conductance in a 3D Ar lattice across a defect plane 50%-filled with periodic array of impurities (rectangles), a uniform defect plane with (pentagons) and without (circles) the second phonon path induced by non-nearest-neighbor bonds, in comparison with that of an atomic plane without defects (hexagons). (b) $\alpha(\omega)$ for a uniform defect plane with (pentagons) and without (circles) the second phonon path.

where $v_{g,z}$ is the phonon group velocity in the cross-plane direction, and $n_{BE}(\omega,T) = [\exp(\hbar\omega/k_B T) - 1]^{-1}$ is the Bose-Einstein distribution of phonons at temperature T. The integral is carried out over the whole Brillouin zone and the sum is over the phonon branches. By embedding defect atoms in a monolayer, we manage to reduce the thermal conductance by 30% in respect to the case of no defects, as shown in Fig. 4(a). This destructive-interference-induced effect can be used to explain the remarkable decrease of the thermal conductivity κ of SiGe alloy with very small amount of Ge, with respect to pristine Si [28]. G can be further reduced by considering the second-nearest-neighbor bonds C_2 between the host atoms on the two sides of the uniform defect layer in addition to the nearest-neighbor bonds C_1 linking the host and adjacent defect atoms; see also Refs. [6,12]. This reduction comes from the suppression of phonon transmission at short wavelengths, shown in Fig. 4(b), which is due to the opening of the second phonon path through the non-nearest-neighbor bonds C_2 interfering destructively with the first path through the nearest-neighbor bonds C_1. The emergence of the second phonon path substantially reduces G, by 16%, despite the weakness of the corresponding bonds: $C_2 = 0.08C_1$ in the Ar lattice [19]. This demonstrates another advantage of the application of the two-path destructive phonon interference for the thermal conductivity reduction: counter-intuitively, more heat flux is blocked by the opening of the additional phonon paths.

In Fig. 5, we report the two-path phonon antiresonance in Si crystal as the metamaterial incorporating 2D planar impurity array of Ge atoms. The Ge and Si atoms have a mass ratio of 2.57 and thus the Ge-atom array introduces both heavy mass and bond defects due to a weaker coupling between Ge:Si than the Si:Si interaction [20].

The nonlinear effects on the two-path phonon interference antiresonance was investigated by increasing the amplitude A of the incident phonon WP, as shown in Fig. 5(b). As A increases, the reflection becomes less pronounced with more heat flux passing through, which provides direct evidence of inelastic phonon scattering at the defect plane. The antiresonances demonstrate a redshift in frequency due to the
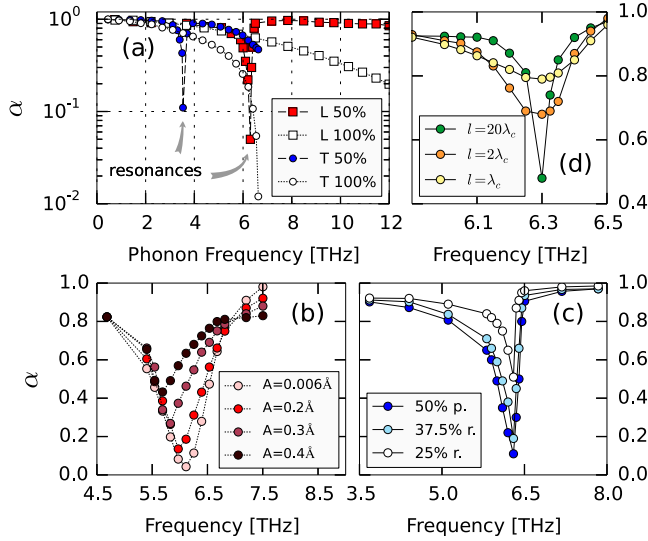
FIG. 5. (Color online) (a) Two-path phonon interference antires-onance for both longitudinal and transverse phonons across a segregated Ge-defect layer (red squares and blue circles) plotted along with the nonresonant transmission across the uniform Ge-defect layer (open squares and circles) in a Si phononic metamaterial. (b) Evolution of the reflection resonance versus the increasing wave amplitude. (c) $\alpha(\omega)$ for a defect layer containing randomly dispersed Ge atoms with $f_d = 37.5\%$ and 25%, compared with that of a defect layer containing 50% of periodically alternating Ge atoms. The measured $\alpha(\omega)$ were averaged over different random distributions. (d) Resonance dip broadening in the limit of small filling fraction $f_d = 5\%$ for WP with a short coherence length ($l = \lambda_c$ and $l = 2\lambda_c$, yellow and orange circles), in comparison with that of almost plane-wave WP ($l = 20\lambda_c$, green circles).

higher-order (cubic) terms in the interatomic potential. We also note in this connection that our computation of a quasi-1D atomic chain containing an impurity atom characterized by nonparabolic (nonlinear) interaction potential with neighbor-ing host atoms agree with our MD results. The interference antiresonance remains pronounced even when the interaction nonlinearity becomes fairly strong. Therefore the two-path phonon interference antiresonance in the proposed phononic metamaterial makes it possible to control thermal energy transport in the case of huge lattice distortions, for instance at very high temperatures.

In contrast to light [29], even a single defect atom in a lattice plane produces interference antiresonance for phonons because of the presence of the two phonon paths. Therefore, phonon reflection should be apparent even for defect-atom arrays in the absence of periodicity because of the localized nature of the resonance. This is supported by further inves-tigating the phonon transmission through the arrays of Ge atoms, distributed in a plane in Si phononic metamaterials with different f_d and randomness. Strong transmission dip, similar to that in periodic arrays, remains pronounced in both

cases, as shown in Fig. 5(c). This was shown experimentally to be equally valid in macroscopic acoustic metamaterials [26].

Chen *et al.* reduced κ below the alloy limit by distributing random Ge segregates in Si superlattices [11]. Their *ab initio* calculations showed that the phonon MFP was substantially reduced in the low frequencies [11]. We note that the Ge segregates can be regarded as randomly dispersed heavy resonators which scatter low-frequency thermal phonons by the interference antiresonances, redshifted according to the isotopic-shift law; cf. Eq. (2). With this destructive inter-ference, we can also explain the extremely low κ found in the $In_{0.53}Ga_{0.47}As$ alloy randomly embedded with heavy ErAs nanoparticles [8].

The decreased 2D defect filling fraction f_d narrows the antiresonance width because of weakening of the relative strength of the "defect-bond" phonon path through the crystal plane; see Fig. 1 and Eq. (1). In general, the width $\Delta\omega$ of the antiresonance dip for our two-path phonon interference is determined by both the f_d and the finite coherence length l of the phonon WP. As follows from Fig. 2, for the large $f_d = 50\%$, $\Delta\omega$ is not sensitive to l. In the limit of small f_d and for $l \gg \lambda_c$, $\Delta\omega$ is narrow and decreases with f_d, as shown in Figs. 5(c) and 5(d). In this limit, for the WP with short $l, l \sim \lambda_c$, $\Delta\omega$ will be determined mainly by l [1]. From Fig. 5(d), the full width at half minimum of the dip for WP with $l = 2\lambda_c$ is $\Delta\omega = 0.19$ THz. Then from the inequality $\Delta\omega\Delta t \geqslant 1/2$, we get the WP width in the time domain $\Delta t = 2.6$ ps and the WP spatial width (coherence length) $l = v_g\Delta t = 3.1$ nm, where $v_g = 1.2$ km/s is the longitudinal phonon group velocity in Si at $\omega = \omega_R$. This length coincides with the WP coherence length of ≈ 3.2 nm, which was used in the MD simulation shown in Fig. 5(d). The width $\Delta\omega$ of the antiresonance dip for the WP with a shorter coherence length $l = \lambda_c$ is larger than that of the WP with $l = 2\lambda_c$; see Fig. 5(d). Therefore the width of the two-path phonon interference dip in the transmission spectrum can provide a measure of the coherence length of the phonon WP, similar to the width of the HOM dip in the two-photon interference [1].

In conclusion, we provide comprehensive modeling of atomic-scale phononic metamaterial for the control of heat transport by exploiting two-path phonon interference an-tiresonances. Thermal phonons crossing the defect plane with the two paths of different nature undergo destructive interference, which results in the reduction of thermal con-ductance. Interference antiresonances are not deteriorated by the aperiodicity in the defect arrays and by the anharmonicity of atom bonds. The width of antiresonance dip provides a measure of the coherence length of the phonon wave packet. Such patterned atomic planes can be considered as high-finesse atomic-scale phononic mirrors. And, finally, we would emphasize that strong optical reflections observed in 3D stereometamaterials [30] can also be interpreted as photon interference antiresonances in an optically transparent plane, embedded with plasmonic nanostructures.

[1] C. K. Hong, Z. Y. Ou, and L. Mandel, Phys. Rev. Lett. **59**, 2044 (1987).

[2] C. Santori, D. Fattal, J. Vuckovic, G. Solomon, and Y. Yamamoto, Nature (London) **419**, 594 (2002).

[3] J. Beugnon, M. P. A. Jones, J. Dingjan, B. Darquie, G. Messin, A. Browaeys, and P. Grangier, Nature (London) **440**, 779 (2006).

[4] C. Lang, C. Eichler, L. Steffen, J. M. Fink, M. J. Woolley, A. Blais, and A. Wallraff, Nat. Phys. **9**, 345 (2013).

[5] S. M. Wang, S. Y. Mu, C. Zhu, Y. X. Gong, P. Xu, H. Liu, T. Li, S. N. Zhu, and X. Zhang, Opt. Express **20**, 5213 (2012).

[6] Yu. A. Kosevich, Prog. Surf. Sci. **55**, 1 (1997).

[7] I. Chowdhury, R. Prasher, K. Lofgreen, G. Chrysler, S. Narasimhan, R. Mahajan, D. Koester, R. Alley, and R. Venkatasubramanian, Nat. Nanotechnol. **4**, 235 (2009).

[8] W. Kim, J. Zide, A. Gossard, D. Klenov, S. Stemmer, A. Shakouri, and A. Majumdar, Phys. Rev. Lett. **96**, 045901 (2006).

[9] N. Mingo, D. Hauser, N. P. Kobayashi, M. Plissonnier, and A. Shakouri, Nano Lett. **9**, 711 (2009).

[10] G. Pernot, M. Stoffel, I. Savic, F. Pezzoli, P. Chen, G. Savelli, A. Jacquot, J. Schumann, U. Denker, I. Mönch, Ch. Deneke, O. G. Schmidt, J. M. Rampnoux, S. Wang, M. Plissonnier, A. Rastelli, S. Dilhaire, and N. Mingo, Nat. Mater. **6**, 491 (2010).

[11] P. Chen, N. A. Katcho, J. P. Feser, W. Li, M. Glaser, O. G. Schmidt, D. G. Cahill, N. Mingo, and A. Rastelli, Phys. Rev. Lett. **111**, 115901 (2013).

[12] Yu. A. Kosevich, Phys. Usp. **51**, 848 (2008).

[13] M. Maldovan, Phys. Rev. Lett. **110**, 025902 (2013).

[14] L. Zhang, P. Keblinski, J. S. Wang, and B. Li, Phys. Rev. B **83**, 064303 (2011).

[15] N. Li, J. Ren, L. Wang, G. Zhang, P. Hänggi, and B. Li, Rev. Mod. Phys. **84**, 1045 (2012).

[16] H. Xu, X. Shi, F. Gao, H. Sun, and B. Zhang, Phys. Rev. Lett. **112**, 054301 (2014).

[17] T. Han, X. Bai, D. Gao, J. T. L. Thong, B. Li, and C.-W. Qiu, Phys. Rev. Lett. **112**, 054302 (2014).

[18] S. Narayana and Y. Sato, Phys. Rev. Lett. **108**, 214303 (2012).

[19] H. Kaburaki, J. Li, S. Yip, and H. Kimizuka, J. Appl. Phys. **102**, 043514 (2007).

[20] F. H. Stillinger and T. A. Weber, Phys. Rev. B **31**, 5262 (1985).

[21] P. Schelling, S. Phillpot, and P. Keblinski, Appl. Phys. Lett. **80**, 2484 (2002).

[22] S. Plimpton, J. Comput. Phys. **117**, 1 (1995).

[23] U. Fano, Phys. Rev. **124**, 1866 (1961).

[24] Yu. A. Kosevich and E. S. Syrkin, Fiz. Tverd. Tela (Leningrad) **33**, 2053 (1991) [Sov. Phys. Solid State **33**, 1156 (1991)].

[25] H. Estrada, P. Candelas, A. Uris, F. Belmar, F. J. García de Abajo, and F. Meseguer, Phys. Rev. Lett. **101**, 084302 (2008).

[26] Z. Liu, X. Zhang, Y. Mao, Y. Y. Zhu, Z. Yang, C. T. Chan, and P. Sheng, Science **289**, 1734 (2000).

[27] I. M. Khalatnikov, *An Introduction to the Theory of Superfluidity* (Benjamin, New York, 1965).

[28] J. Garg, N. Bonini, B. Kozinsky, and N. Marzari, Phys. Rev. Lett. **106**, 045901 (2011).

[29] A. Degiron, H. Lezec, N. Yamamoto, and T. Ebbesen, Opt. Commun. **239**, 61 (2004).

[30] N. Liu, H. Liu, S. Zhu, and H. Giessen, Nat. Photonics **3**, 157 (2009).